2012

Small Scale Simulation Chamber for Space Environment Survivability Testing

Robert H. Johnson
Utah State University

Lisa D. Montierth
Utah State University

JR Dennison
Utah State Univesity

James S. Dyer

Ethan Lindstrom

Alex Chanson

Small Scale Simulation Chamber for Space Environment Survivability Testing

Robert H. Johnson, Lisa D. Montierth, JR Dennison
James S. Dyer, Ethan Lindstrom, and Alex Chanson

***Abstract*— A versatile vacuum system for long duration testing of materials modifications due to exposure to simulated space environment conditions has been designed and built. The chamber is particularly well suited for cost-effective tests of multiple small scale materials samples over prolonged exposure. Critical environmental components simulated include neutral gas [ultrahigh vacuum (10^{-7} Pa) to ambient], FUV/UV/VIS/NIR solar spectrum, electron plasma fluxes, and temperature. The UV/VIS/NIR solar spectrum is simulated using an external, normally incidence and collimated class AAA Solar Simulator source, with standard Air Mass Zero (AM0) filters to shape the incident radiation spectrum. This Xe arc discharge tube source has a 200 nm to 2000 nm range with up to four suns light intensity capability. Light intensity feedback is used to maintain the intensity temporal stability during the sample exposure cycle, with standard calibrated solar cells mounted internally on the sample mounting block. Incident FUV (far ultraviolet) intensity radiation is provided by Kr discharge line sources, with a primary emission line at 124 nm and secondary emission line at 117 nm with up to four suns intensity. This provides an adequate substitution for the solar FUV spectrum, which is dominated by the ultraviolet hydrogen Lyman α emission line at 122 nm. An electron flood gun provides a uniform, monoenergetic (~20 eV to ~15 keV) electron flux. Electron fluxes at the sample surface of <1 pA-cm^{-2} to >1 μA-cm^{-2} are continuously monitored during the sample exposure cycle, using a standard Faraday cup mounted on the sample block. The chamber maintains ≤98% uniformity of the electromagnetic and electron radiation exposure over a sample area of ~70 cm^2. Samples are mounted on a rotatable OFHC Cu sample block with large thermal mass to minimize the differences in temperature between samples and thermal fluctuations during the sample exposure cycle. A controlled, uniform temperature range from 100 K to 450 K is achieved using a cryogenic reservoir and resistance heaters attached to the sample block. The sample carousel is attached to a standard rotational vacuum feedthrough, to allow 355° rotation of the samples relative to the incident fluxes. Reflectivity and emissivity are measured by extending a compact integrating sphere with a fiber optic connection to an external calibrated commercial UV/VIS/NIR spectrometer and an IR absorptivity/emissivity probe mounted on a linear translation stage toward the center of the chamber; each sample and in situ calibration standards are rotated under the probes in turn. An automated data acquisition system periodically monitors and records the environmental conditions, UV/VIS/NIR reflectivity, and IR emissivity of the samples in situ during the sample exposure cycle.**

***Index Terms*—materials testing, space environment, instrumentation**

.

I. Introduction

The space environment can modify materials and cause detrimental effects to satellites. Some of these effects are change in reflectivity and emissivity, which lead to changes in thermal, optical, and charging properties. If these are severe enough the spacecraft will not operate as designed.

The key to predicting and mitigating these deleterious effects is the ability to accurately simulate space environment effects through long-duration, well-characterized testing in an accelerated, versatile laboratory environment.

There are certain characteristics of the space environment that are critical for a true simulation. These critical characteristics are electron flux, electromagnetic radiation, vacuum, and temperature. The electron flux is critical because the solar winds through space bombard spacecraft. The electromagnetic radiation has many critical aspects in itself. As can be seen in figure 10, the sun has a very broad range covering from the Visual/Infrared to Ultra Violet, specifically the Hydrogen Lyman Alpha emission at 121.6 nm. A vacuum simulation is critical because space is a vacuum, meaning very few particles. The temperature is critical because it changes drastically depending on proximity to the sun. Things not covered by this chamber are photons/ions, and atomic oxygen.

II. Space Simulation Capabilities

Research was supported by funding from the Utah State University Space Dynamics Laboratory.

Robert Johnson and JR Dennison are with the Materials Physics Group in the Physics Department at Utah State University in Logan, UT 84322 USA (e-mail: Motojunker@yahool.com, JR.Dennison@usu.edu). Lisa Montierth, Jim Dyer, and Ethan Lindstrom work with the ??? division in the Utah State University Space Dynamics Laboratory University in North Logan, UT 843?? USA (e-mail: ???). Johnson and Montierth are undergraduate students in the Mechanical Engineering Department, Utah State University. Alex Chanson is an undergraduate student in the Physics Department, University of California-Berkeley.

.

Fig. 1. Front (Left) and side (Right) views of a Lichtenberg discharge tree. The white line (Right) indicates the narrow distribution of deposited charge from a ~1 MeV electron beam at R≈3 mm in a PMMA sample.

The desired range expression can be developed by merging well known semi-empirical models for the interaction of electrons with materials in different energy regimes by employing the continuous-slowing-down approximation (CSDA). In the CSDA, the rate of energy loss, (or total stopping power, S_{CSDA}), at every position along the penetration path is assumed constant; variations in energy-loss rate with energy, E, or penetration depth, z, are neglected. For a given incident energy, E_b, the CSDA range is obtained by integrating total stopping power over the full penetration depth such that [1, 2].

In the CSDA with a constant energy-loss rate,

— (1)

Here is equal to mean energy lost per collision occurring at mean free path , and E_{min} is the energy at the minimum in the inelastic mean free path curve at $\lambda_{min} \equiv \lambda_{IMFP}(E_{min})$. A reasonable approximation for is the geometric mean of the effective plasmon energy and the bandgap energy, E_{gap}, times an empirically determined factor of 2.8 [3]:

(2)

The effective plasmon energy, , for an arbitrary atomic or molecular material is defined in analogy with the bulk free-electron plasma energy for conductors—which is proportional to the square root of the number of valance electrons per atom or molecule—as

(3)

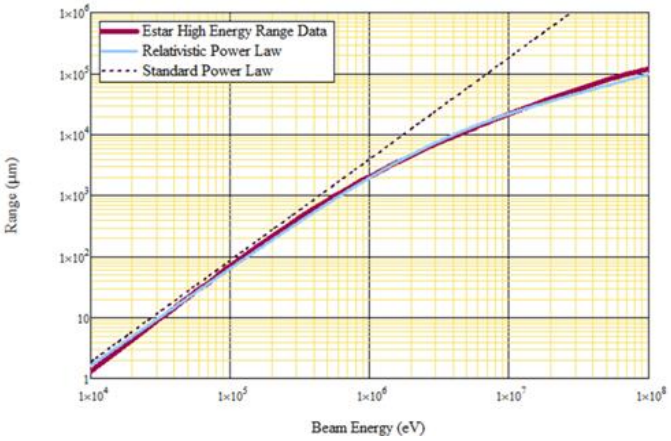

Fig. 2. Comparison between the standard power law and the relativistic power law for Al. The relativistic power law allows approximations for energies up to 10 MeV with percent errors ~20%.

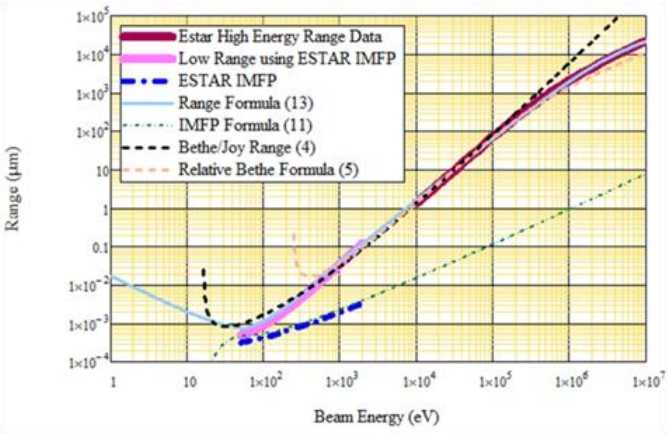

Fig. 3. Comparison between several range approximations and the data from the ESTAR database for Al [4]. The IMFP data for Al are also plotted, along with the TPP-2M IMFP formula for $\lambda_{IMFP}(E)$ [5].

Following the analogy, the free parameter is termed the effective number of valence electrons per atom, as discussed further below. Here q_e and m_e are the electron charge and rest mass, $\hbar$ is the reduced Planck's constant, ε_0 is the permittivity of free space, N_A is Avogadro's number, M_A is the atomic weight, and ρ_m is the mass density [4].

Tabulated values of the electron ranges at high energies using the CSDA can be found in the NIST ESTAR database spanning incident energies from E_{HI}~20 keV to ~1 GeV [5].

The CSDA can also be applied to lower energy ranges. The NIST electron inelastic mean free path (IMFP) database [6] has tabulated values and semi-empirical fits for the IMFP—which is closely related to the range as shown below—which are valid for energies from ~30 eV to E_{LO}~1 keV.

Thus, in order to create an analytic expression for the full span of desired energies, the problem can be broken into three parts according to energy of the incident electron: a high energy range for $E_b > E_{LO} \equiv 1$ keV; a mid-energy range for $< E_b < E_{LO}$; and a low energy range for energies $E_b <$.

A. High Energy Range

Range values at high energy are tabulated in the NIST ESTAR database [5]. The non-relativistic Bethe-Joy range expression based on the Bethe stopping power formula [7] has been extended to lower energies by Joy and Luo [8] and Tanuma [9], with the addition of a fixed empirical constant,

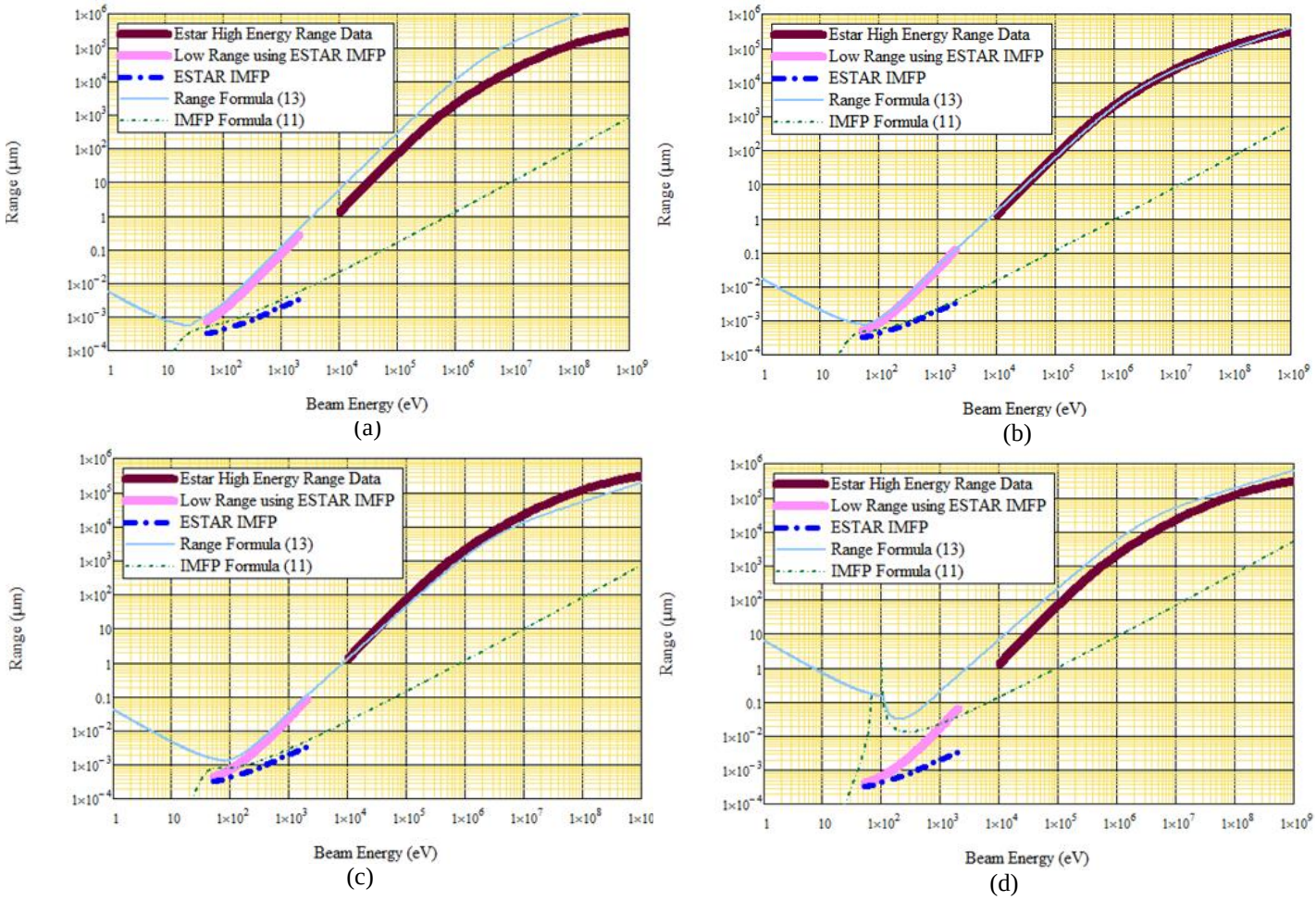

Fig. 4. Graphs showing the variation of the range expression for Al, as a function of the single fitting parameter . For graphs (a) through (d), = 1, 5 (best fit), 10 and 18, respectively.

k=0.8 and by replacing the mean excitation energy, J, in the Bethe expression with a closely related empirical parameter, J_{exp}. The resulting Bethe-Joy-Luo expression

(4)

is used to fit the data up to ~10^5 eV, above which a relativistic correction becomes significant [10]. Z_A is the atomic number and we have replaced the Joy-Luo empirical parameter J_{exp} with our empirical parameter . A relativistic extension of this equation is

(5)

A common approximation for $R(E_b)$ for ~1 keV<E_b<50 keV is a simple power law formula, with a stopping power exponent n;

(6)

where in the non-relativistic limit, the incident free electron energy is . In general, physical constraints require $0 \le n \le 1$ [1]. Numerous power law models have been developed for different classes of materials, with $0.35 \le n \le 0.67$ [1 and references therein]. Indeed, Eq. (4)—in the limit where the $ln(E_b)$ term is negligible—reduces to a limiting-case Thomson-Whiddington n=1 power law dependence [11].

A simple power law approximation applicable to higher incident energies is found by inserting the relativistic velocity equation into Eq. (6):

(7)

Above ~10 MeV (higher energies for lower Z_A materials), total bremstrahlung radiation energy losses—proportional to E^2 using the Kramers efficiency relation—dominate energy losses due to collisions. Figure 2 shows the fit to tabulated data for Al from the ESTAR database, using both non-relativistic and relativistic power law expressions, Eqs. (6) and (7), respectively. Figure 3 shows fits to the Al data using several range approximation formulas.

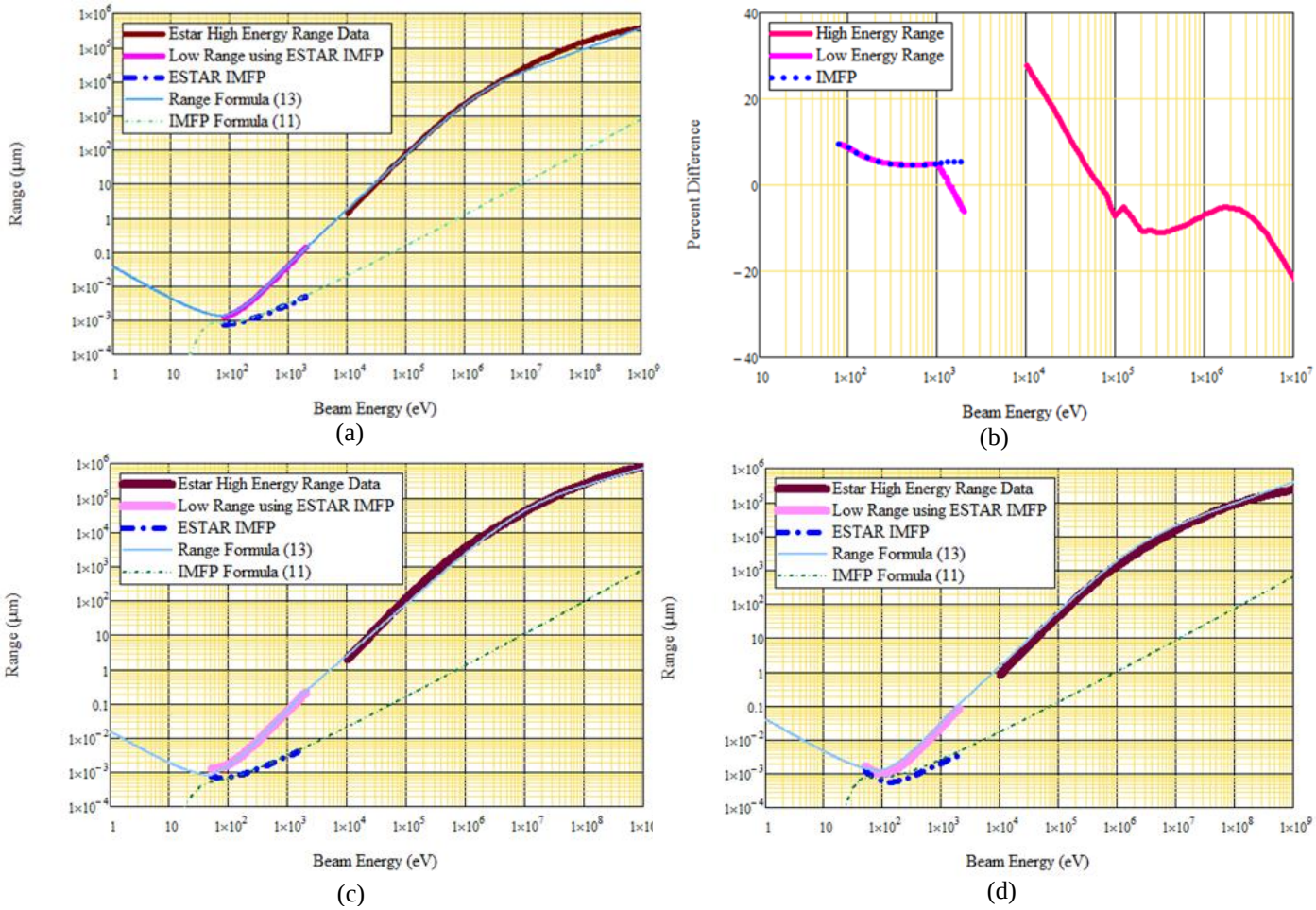

Fig. 5. (a) Comparison of the range formula for SiO_2 with = 6.0 . (b) Residual plot of SiO_2 range data in Fig 5. (c) Comparison of the range formula for Kapton with =2. (d) Comparison of the range formula for Al_2O_3 with =5.0.

The stopping power exponent n and proportionality constant b can be expressed in terms of by matching the slope and magnitude of the approximate power law formula, Eq. (6) or (7), to the Bethe-Joy-Luo and mid-energy range expressions, respectively. n is determined by requiring that the slope of the range power law from Eq. (6) for $R_{HE}(E)$ matches the Bethe-Joy-Luo formula—Eq. (4)—at two non-relativistic energies, E_{LO} and E_{HI}, in the regime where both expressions give reasonable results. $E_{HI}\equiv 20$ keV is the lower energy at which data are available for all materials in the ESTAR database and $E_{LO}\equiv 1$ keV is the upper energy at which data are available for all materials in the IMFP database. This leads to an expression for the stopping power exponent

(8)

The magnitude of the high energy range expression, Eq. (7), is normalized to the mid-energy expression—Eqs. (10) and (11) developed in Section B—at E_{LO}, by setting

(9)

Note that the only free parameter in Eqs. (8) and (9) is , along with which is expressed in terms of and the band gap energy, E_{gap} in Eq. (1).

B. Mid-Energy Range

Direct extrapolation of the range from the ESTAR data to lower energies is not valid for energies comparable to the atomic electronic structure, typically a few keV and below, because the discrete energy nature of the collisions becomes important. However, a simple extension of the CSDA to lower energies can relate the range to the electron IMFP, where

(10)

Here the stopping power is again assumed equal to the total energy lost (incident energy, E_b) divided by the total distance traveled (range, $R(E_b)$). This is set equal to the mean energy lost per collision, , divided by the mean distance traveled per collision all times the probability that a collision occurs,

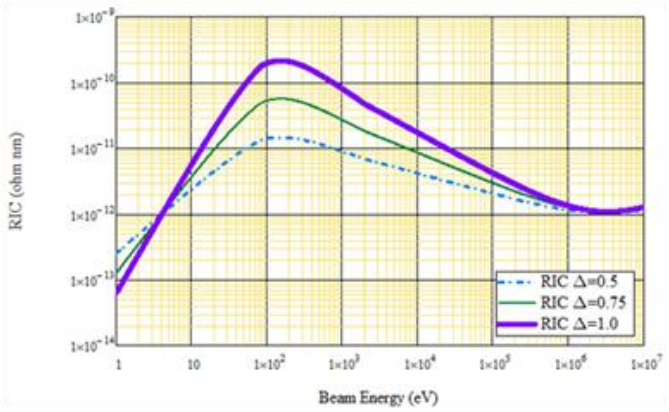

Fig. 7. RIC as a function of energy in the CSDA for polyimide.

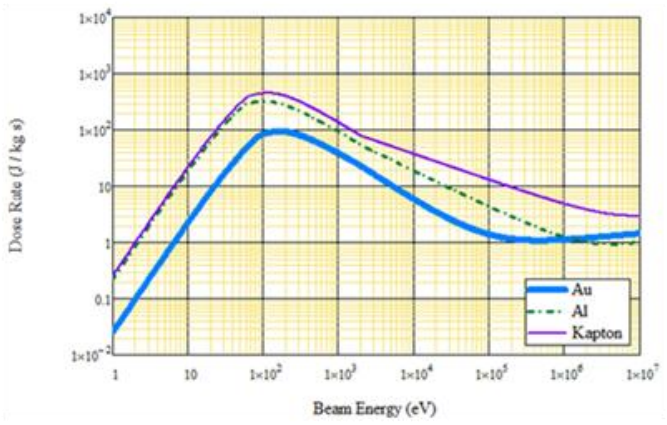

Fig. 6. Dose rate as a function of energy in the CSDA for Au, Al and polyimide .

= . For $>E_b>E_{HI}$, $\lambda_{IMFP}(E_b)$ is assumed to be given by the TPP-2M formula [12] used in conjunction with the NIST IMFP database [6]:

(11)

where (12)

Because of the shallow core levels (generally with binding energies <30 eV) that may contribute significant intensity to the energy-loss function, there arises an ambiguity in the choice of the value of the number of valence electrons [12]. Powell *et al*. used the bulk free-electron plasma energy value for in Eq. (12) for elemental conductors, and obtained good agreement with optical absorption and inelastic electron scattering data which are often described in terms of a parameter termed the "effective number of electrons per atom" [9,12,13]. Powell *et al*. also found good agreement for studies of other materials, including, semiconductors, insulators, and organic and inorganic compounds, by determining the parameter from sum rule considerations of the scattering contributions from electrons in particular atomic shells or subshells [9,12,13]. There are extensive discussions on the best way to approximate these fitting parameters, based solely on materials properties [8,12,14]. Gries used an alternate approach to model the IMFP, based on empirical fits and an "effective Z parameter", Z^*, described as the "nominal effective number of interaction-prone electrons per atom" [14]; note, however, that Tunuma, Powell and Penn took exception to the physical interpretation of this fitting parameter [12].

IMFP data from the NIST database [6] (see thick blue dashed curves in Figs. 3, 4 and 5) were fit well over the mid-energy range using the TPP-2M model given by Eqs. (11) and (12) with determined by fits to the ESTAR database [5] through Eqs. (8) and (9) (see thin dashed green curves in Figs. 3, 4 and 5). Once again, by using the proposed TPP-2M equations of Tanuma inserted into Eq. (10), the only free parameter for the mid-energy range expression is , along with the materials constants E_{gap}, M_A, and ρ_m through . While E_{gap} may be considered an additional fitting parameter for semiconductors and insulators, its effect on R is minimal, causing primarily a vertical shift in the range curve within 2% using acceptable band gap energies. Thus, E_{gap} can be treated essentially as an additional tabulated material constant—such as M_A and ρ_m are—derived from independent optical measurements.

C. Low Energy Range

To calculate the range for $E_b<$, we assume in the CSDA that: (i) the energy lost per low energy collision is constant and equal to the mean excitation energy, ; (ii) the IMFP is constant and equal to the IMFP at the mean energy loss or $\lambda_{IMFP}( )=$; and (iii) the probability that an electron undergoes one such inelastic collision falls off as = . This simple low energy approximation avoids the unusual asymptotic behavior exhibited by the TPP-2M expression at energies below that is evident in the thin dashed green curves in Figs. 3, 4, and 5. The resulting expression is consistent with a universal curve of electron IMFP versus kinetic energy [15] observed for a wide range of materials [16], that is consistent with a simple free electron gas model of valence electrons in the material [17].

D. Composite Range Function

The final result is a continuous composite analytic approximation to the range, spanning from <10 eV to >10 MeV, with a single fitting parameter, :

(13)

Figure 4 demonstrates the sensitivity of the composite fit, Equation (10), to for a typical conductor, Al. Lower values of overestimate the range, while higher values of

Table I. Materials Properties and Fitting Parameters

Material		Fitting Parameter	Material Properties				Derived Values				
Name	Formula		ρ_m (gm/cm^3)	Z_A	M_A (amu)	E_{gap} (eV)	n	b (μm/eV^n)	(eV)	E_m (eV)	λ_{min} (nm)
Graphite	C	5.3	1.7	6	12.01	0.1	0.642	0.7143	24.87	69.6	0.793
Amorphous C	C	4.0	2.0	6	12.01	0.1	0.676	0.3877	23.43	65.6	0.614
Aluminum	Al	5.0	2.7	13	26.98	0.0	0.668	0.5075	20.31	56.9	0.467
Silicon	Si	5.0	2.33	14	28.09	1.11	0.676	0.5422	18.49	51.9	0.438
Copper	Cu	8.3	8.96	29	63.55	0.0	0.561	0.7821	31.06	87.0	0.422
Germanium	Ge	9.8	5.32	32	72.64	0.66	0.571	1.355	24.32	68.1	0.477
Silver	Ag	10.6	10.5	47	107.87	0.0	0.536	1.217	29.17	81.7	0.416
Gold	Au	12.0	19.32	79	196.97	0.0	0.508	1.261	31.15	87.2	0.371
Polyethylene	$[C_2H_4]_n$	2.5	0.94	2.65	4.64	2.9	0.727	0.2354	20.43	57.8	0.642
Polyimide	$[C_{22}H_{10}N_2O_5]_n$	4.1	1.42	5.01	9.769	2.3	0.678	0.4582	22.17	62.4	0.652
PTFE	$[C_2F_4]_n$	6.0	2.2	8.01	16.023	6	0.620	0.8794	26.06	78.9	0.865
Aluminum Oxide	Al_2O_3	5.0	3.97	10	30.392	9.9	0.628	0.5188	28.33	84.0	0.746
Silicon Dioxide	SiO_2	6.0	2.32	9.98	19.99	8.9	0.622	0.895	23.90	71.4	0.818
Glass, Pyrex	doped SiO_2	6.2	2.32	9.98	19.99	4	0.626	0.8150	24.36	69.1	0.656

underestimate the range. Based on the quality of the fits to the database values, the typical uncertainty in is estimated to be 10%. The residual curve for the fit for Al is shown in Fig. 5(b).

Figures 5(a), 5(c) and 5(d) show best fits to data for three prototypical materials: the conductor Al; the polymeric insulator polyimide (Kapton), and the insulating ceramic Al_2O_3. Table I lists the fitting parameter , along with materials properties and derived values, for 14 common spacecraft materials. A more extensive set of fitting parameters for additional materials is currently being developed.

III. Applications

The usefulness of an analytical approximation of the range to spacecraft applications can easily be demonstrated by considering expressions for the dose rate and the radiation induced conductivity; both expressions require an energy dependent range expression.

The dose rate, , is defined as the power deposited by incident radiation per unit mass. The dose rate in the CSDA for a homogeneous material is inversely proportional to the volume in which radiation energy is deposited; this volume is approximately equal to the beam cross sectional area times R [18]. Thus,

(14)

The dose rates for three materials as a function of incident energy are shown in Fig. 6.

Radiation Induced Conductivity (RIC) is the enhanced conductivity that results from the energy deposited in this volume. In the CSDA

(15)

with ½<Δ<1 [19]. Figure 7 shows the RIC for Kapton as a function of incident energy for three values of Δ. As expected, RIC effects are generally larger for larger Δ, with the variation largest at the maximum value near 3 and becoming much smaller in the relativistic region. The magnitude of RIC exhibits a crossover at~2 eV; however, this is below the energy range for which Equation 10 is valid.

Notice that both and σ_{RIC} exhibit energy dependent maxima as a consequence of the minimum in the range expression. Both curves also have local minima at ~3 MeV for Au, as a result of the relativistic correction in Eq. (7) that occurs at lower energies for more dense materials.

Secondary electron (SE) emission is another electron scattering process for which application of the range expression developed here could provide insight. In the CSDA, the SE yield can be expressed as [1]

(16)

In a similar vein, Yasuda *et al.* have investigated the SE yield in terms of the relation between the IMFP and the valence electron excitation function (which they approximate by the outer shell ionization function) [20]. Earlier, Ashley and Williams found that the electron stopping power for many polymers was a function of the ratio of the number of valence electrons, N_v, in a monomer unit to its molecular weight, M_A [21]. Burke used their relation to express the secondary electron emission coefficient from polymers as a function of N_v / M_A in a semi-empirical model [22]. Work is underway at USU to develop an expression for the SE yield in terms of the composite range expression, Equation (10). The resulting SE expression would have three independent free parameters; N_V and the maximum SE yield δ_{max} at energy E_{max}.

IV. CONCLUSION

Using the CSDA, a continuous, simple, composite, analytic formula—with a single free parameter, termed the effective number of valence electrons, —has been developed to approximate the range (10^{-9} m to 10^{-2} m) over an extended energy span (<10 eV to >10 MeV). Agreement with available databases of electron interactions are within <20% for many

conducting, semiconducting, and insulating materials. Use of this continuous expression over the extended energy range permits development of continuous expressions over extended energy ranges for dose rate, RIC and (potentially) SE yield. By comparing these extended expressions to data, which are often considerably easier to measure than range, the range formula can be further validated and improved. Continued development may also establish the ability to approximate the fitting parameter, , using only material and empirical constants. This would allow construction of an empirical database for materials without the necessity of specific range data.

REFERENCES

1. Reimer, L., 1998, "Scanning Electron Microscopy: Physics of Image Formation and Microanalysis," 2nd Ed., Springer-Verlag,Heidelberg.
2. Spencer, L., 1955, "Theory of Electron Penetration," Phys. Rev. 98, 1597.
3. Alig, R., and S. Bloom, 1975, "Electron-Hole-Pair Creation Energies in Semiconductors," Phys. Rev. Lett. 35, 1522.
4. Pines, D., 1963, *Elementary Excitations in Solids*, Addison-Wesley, Reading, MA.
5. National Institute of Standards and Technology, 2010, "ESTAR, Stopping Power and Range Tables for Electrons," (http://physics.nist.gov/PhysRefData/Star/Text/ESTAR.html).
6. National Institute of Standards and Technology, 2010, "NIST Electron Inelastic-Mean-Free-Path Database: Version 1.1," (http://www.nist.gov/data/nist71.htm).
7. Bethe, H., and W. Heitler, 1934, "On the Stopping of Fast Particles and on the Creation of Positive Electrons," in Proc. Royal Soc. London. Series A, Containing Papers of a Mathematical and Physical Character 146, 83.
8. Joy D.C., and Luo S., 1989, "An empirical stopping power expression for low energy electrons," Scanning 11, 176.
9. Tanuma, S., C. Powell, and D. Penn, 2005, "Calculations of Stopping Powers of 100 eV to 30 keV Electrons in 10 Elemental Solids," Surf. Inter. Anal. 37, 978.
10. Evans, R.D., 1955, *The Atomic Nucleus*, Internat. Ser. In Pure and Appl. Phys., McGraw-Hill, New York.
11. Whiddington, R., 1914, "The Transmission of Cathode Rays Trough Matter," in Proc. Royal Soc. London. Series A, Containing Papers of a Mathematical and Physical Character 89, 554.
12. Tunuma, S, C.J. Powell and D.R. Penn, 1997, "Calculations of Electron Inelastic Mean Free Paths (IMFPs) VI. Analysis of the Gries Inelastic Scattering Model and Predictive IMFP Equation," Surf. Inter. Anal. 25, 25.
13. Powell, C.J., and A. Jablonski, 2000, "Evaluation of Electron Inelastic Mean Free Paths for Selected Elements and Compounds," Surf. Inter. Anal. 29, 108-114.
14. Gries, W.H., 1996, "A Universal Predictive Equation for the Inelastic Mean Free Pathlengths of X-ray Photoelectrons and Auger Electrons," Surf. Inter. Anal. 24, 38.
15. Zangwill, A., 1988, *Physics at Surfaces*, Cambridge Univ. Press, New York.
16. Somorjai, G.A. , 1981, *Chemistry in Two Dimensions: Surfaces*, Cornell Press, Ithica.
17. Penn, D.R. , 1976, "Electron Mean Free Paths for Free-electron-like Materials," Phys. Rev B, 13 5248.
18. Roth, J.A., R. Hoffmann, and J.R. Dennison, 2009, "Effects of Radiation Induced Conductivity on Electrostatic Discharge in Insulating Materials," in Proc. 1st AIAA Atmospheric and Space Environments Conf. (San Antonio, TX).
19. Dennison, J.R., J. Gillespie, J.L. Hodges, R.C. Hoffmann, J. Abbott, A.W. Hunt and R. Spalding, "Radiation Induced Conductivity of Highly-Insulating Spacecraft Materials," in *Application of Accelerators in Research and Industry*, Am. Instit. Phys. Conf. Proc. Series, Vol. 1099, ed. F.D. McDaniel and B. L. Doyle, (Am. Instit. of Phys., Melveille, NY, 2009), pp. 203-208.
20. Yasuda, M,. T. Nobuo and H, Kawata, 2004, "A Monte Carlo Calculation of Secondary Electron Emission from Organic Compounds," Jap. J. Appl. Phys., 43, 4004–4008.
21. Ashley, J. C. and M. W. Williams, 1980, "Electron Mean Free Paths in Solid Organic Insulators," Radiat. Res. 81, 364.
22. Burke E. A.,1980, "Secondary Emission from Polymers," IEEE Trans. NS, 27, 1760.

Greg Wilson received dual B.S. degrees in physics and mathematics from Utah State University in Logan, UT, where he is currently a graduate student in physics. He has worked with the Materials Physics Group for two years on electron emission and luminescence studies related to spacecraft charging.

J. R. Dennison received the B.S. degree in physics from Appalachian State University, Boone, NC, in 1980, and the M.S. and Ph.D. degrees in physics from Virginia Polytechnic Institute and State University (Virginia Tech), Blacksburg, in 1983 and 1985, respectively. He was a Research Associate with the University of Missouri—Columbia before moving to Utah State University (USU), Logan, in 1988. He is currently a Professor of physics at USU, where he leads the Materials Physics Group. He has worked in the area of electron scattering for his entire career and has focused on the electron emission and resistivity of materials related to spacecraft charging for the last two decades.